Mater. Res. Soc. Symp. Proc. Vol. 1084 © 2008 Materials Research Society 1084-S03-02

CO Coverage Effects on Pt(111) from First-Principles Calculations

Bin Shan, Ligen Wang, Jangsuk Hyun, Yang Sang, Yujun Zhao, and John B Nicholas
Nanostellar Inc, 3696 Haven Ave, Redwood City, CA, 94063

ABSTRACT

CO saturation coverage on Pt(111) is crucially important in diesel oxidation catalysis. We systematically studied high coverage CO adsorption on the Pt(111) surface using density functional theory (DFT) calculations and classical Monte Carlo (MC) simulations. The zero-coverage limit CO adsorption energy at different binding sites is almost degenerate at the revised Perdew–Burke–Erzernhof functional (RPBE) level. As CO populates the surface, strong through-space repulsion and substrate-mediated metal sharing tends to dominate the stability of adsorbates and alter their binding preferences. The calculated differential binding energy curve and adsorption patterns compare well with experiments.

INTRODUCTION

CO adsorption on Pt surfaces is one of the fundamental steps in diesel engine oxidation catalysis. One of the key parameters that determine the reaction kinetics is CO saturation adsorption. There have been many experimental determinations of CO saturation coverage. However, due to various experimental conditions employed, estimates range from 0.5 monolayer (ML) to 0.7 ML [1-6]. For example, LEED measurements report a saturation coverage of 0.68 ML [1] and 0.71 ML [2], while both electron energy loss spectroscopy (EELS) studies [3] and STM studies [4] indicate adsorbed CO saturates at 0.50 ML with a c(4x2) structure. High pressure STM measurements indicate CO coverage up to 0.7 ML [5,6].

On the theoretical side, CO binding energies have been explored on the many transition metal surfaces [3,7-11]. In particular, CO adsorption on Pt(111) surface has been extensively studied [7,9-11]. The accuracy of different exchange-correlation functionals in predicting CO energies on different adsorption sites was also evaluated [8,12]. Experimental results indicate that at low coverage, CO prefers to bind to atop sites while DFT calculations consistently predict that CO prefers adsorption at hollow sites. The discrepancy is generally attributed to the over estimation of the HOMO-LUMO gap of CO [8,12,13]. A number of theoretical methods have been proposed to correct this problem [13]. Few studies have investigated the CO adsorption at high coverage limit. Hafner et al. [14] have studied CO adsorption with pre-covered CO molecules, but only with a limited set of adsorption configurations.

Under realistic diesel operating conditions, the surface is initially saturated with CO molecules. We thus sought to determine the saturation coverage of CO on Pt(111) surface via DFT calculations [15]. Combining DFT calculations and classical Monte-Carlo (MC) techniques, we have theoretically determined the CO differential binding energy curve and saturation coverage, which agree well with experiments.

COMPUTATIONAL METHODS

The DFT calculations were done using the Vienna Ab-initio Simulation Package (VASP) [17], where Kohn-Sham single-electron wavefunctions are expanded by a series of plane waves. The interactions between ions and valence electrons are described using the projected augmented wave (PAW) method [18] with an energy cut off of 400 eV, at which the CO binding energies are converged to a few meV. We used the revised Perdew–Burke–Erzernhof functional (RPBE) [16] functional, which produces good agreement with experimental adsorption energy values for a number of molecules on transition metal surfaces [16]. The CO binding energies were calculated as the difference in total energy between the optimized Pt-CO complex and the sum of the energies of the optimized bare surface and gas phase CO molecules:

$$\Delta E = E_{total} - (E_{slab} + nE_{CO})$$

In order to probe complex CO equilibrium adsorption geometries at intermediate coverages, we used a *p*(4x4) unit cell (16 surface Pt atoms), with a 2x2x1 k-point mesh to sample the Brillouin zone. The *p*(4x4) unit cell enables us to map out the differential binding energy curve in increments of 0.06 ML from 0.25 to 1.0 ML coverage. The Pt(111) substrate is modeled by a three-layer metal slab separated by a vacuum layer thickness of approximately 15 Å. The bottom layer of the slab is fixed in its crystallographic positions while the other atoms are free to relax [7,9,10,19]. We consider the geometry fully relaxed when the force on each atom is less than 0.03 eV/ Å. The Pt-C and C-O IR stretch frequencies were calculated by diagonalizing the mass weighted second derivative force matrix.

For a *p*(4x4) unit cell, there are 96 total binding sites; 16 atop, fcc, and hcp sites, and 48 bridge sites. To more efficiently explore the configuration space of CO adsorption and locate the global minimum, we used classical Monte Carlo simulations with the Metropolis algorithm [20] and a simulated annealing [21] protocol. Parameters for the classical potential used in the MC calculations were obtained by fitting the DFT data in an iterative process (see below). The MC simulations used periodic boundary conditions and were run multiple times for ten million steps. Below we mostly focus on the lowest energy state at each coverage.

DISCUSSION

Figure 1a shows the four types of CO binding sites on a non-defected Pt(111) surface. With the RPBE functional, the energy differences between different adsorption sites are less than 0.05 eV. These small differences are quickly washed out at higher CO coverage by stronger interactions, such as CO repulsions and metal sharing effects. Thus, the subtle error in CO binding energy under zero coverage limit does not affect our conclusions for high coverage.

We used a classical model to predict low energy configurations. The classical model was initially fitted to DFT binding energies at 0.25, 0.50, 0.75 and 1 ML coverage. Table I lists the calculated CO binding energies for each of these cases as well as Pt-C and C-O bond lengths. The corresponding geometries are shown in figure 2a. The average binding energy of CO decreases with increasing coverage, while the Pt-C bond lengthens. The C-O bond length in the isolated CO molecule at the DFT/RPBE level is 1.1436 Å.

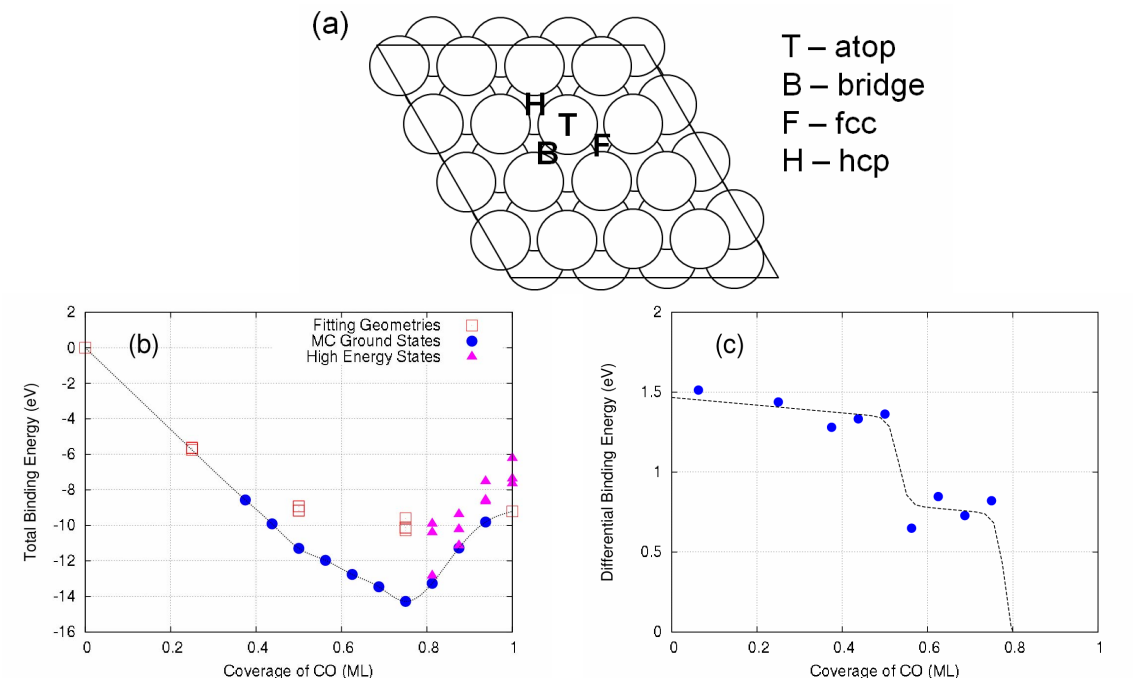

Figure 1. a) Adsorption sites on a Pt(111) surface. b) Total binding energy curve of CO/Pt(111). c) Differential binding energy curve of CO/Pt(111).

Table I. Calculated average CO adsorption energies and bond lengths at 0.25, 0.5, 0.75, and 1 ML coverage.

Adsorption Geometry	Coverage (ML)	Average Adsorption Energy (eV)	Pt-C bond distance (Å)	C-O bond distance (Å)
Top	0.25	-1.404	1.846	1.158
Bridge	0.25	-1.413	2.030	1.181
Fcc	0.25	-1.439	2.128	1.196
Hcp	0.25	-1.414	2.089	1.194
Top	0.50	-1.113	1.848	1.161
Bridge	0.50	-1.133	2.031	1.175
Fcc	0.50	-1.144	2.161	1.186
Hcp	0.50	-1.113	2.115	1.186
Top	0.75	-0.855	1.854	1.160
Bridge	0.75	-0.833	2.046	1.179
Fcc	0.75	-0.840	2.121	1.182
Hcp	0.75	-0.799	2.126	1.182
Top	1.0	-0.575	1.860	1.160
Bridge	1.0	-0.471	2.066	1.172
Fcc	1.0	-0.461	2.151	1.179
Hcp	1.0	-0.389	2.152	1.178

We initially fitted to the 16 DFT data values discussed above to a classical potential energy functional of the following form

$$E_{tot} = n_A \Delta E^0_{top} + n_B \Delta E^0_{bri} + n_F \Delta E^0_{fcc} + n_H \Delta E^0_{hcp} + \frac{1}{2}\sum_{i,j}^{N} \alpha \exp[-\beta(R_{ij} - r_0)]$$

where ΔE^0 represents the low-coverage CO binding energies at the atop, bridge, fcc, and hcp sites, and the through-space repulsions between adsorbates are approximated by an exponential term. R_{ij} is the distance between the carbons in CO. Since CO adsorption is perpendicular to the surface, it makes little difference if we use other distance measures. By setting r_0 to the nearest neighbor distance of Pt (2.821 Å), α represents the energy of the CO-CO interaction at nearest lattice distance. We initially used ΔE^0 values directly from the DFT calculations and fitted the exponential term. The resulting model (Model I, Table 1) fits the DFT data with an R^2 of 0.985 and an RMS of 0.23 eV.

In Model II, binding energies are allowed to vary. The parameters change only slightly from those of Model I. The R^2 improves to 0.996 and the RMS decreases to 0.12 eV. In Model II atop binding energy becomes slightly favored over that of the other sites, consistent with experimental observation. Both models reasonably reproduce the low energy states of CO adsorption.

Table II. Classical potential energy function parameters, binding energies, α (eV) and β (Å). The R^2 and RMS of the resulting fit to the DFT data are included.

	ΔE_{top}	ΔE_{bri}	ΔE_{fcc}	ΔE_{hcp}	α	β	R^2	RMS
Model I[a]	-1.404	-1.413	-1.439	-1.414	0.284	2.980	0.985	0.226
Model II[b]	-1.442	-1.429	-1.433	-1.395	0.292	2.976	0.996	0.120
Model III[c]	-1.418	-1.479	-1.462	-1.423	0.281	2.910	0.994	0.185
δ	/	0.012	0.007	0.009				

a) Using DFT Δ*E*. b) Fitting all parameters. c) Including metal sharing terms.

The parameters of Model II were used in MC simulations to find the lowest energy configuration at intermediate coverages between 0.25 ML and 1 ML. For all the simulations, we kept the two or three lowest energy configurations and refined their energies with DFT calculations. The binding energies predicted by the MC simulations and the corresponding DFT energies usually agree within 0.02 eV/molecule. The R^2 between the Model II MC and DFT energies is 0.99. The simple model does an excellent job of predicting the DFT energies. A linear fit between the two data sets ($E_{MC} = m(E_{DFT}) + b$) gives a slope of 0.993 and intercept of -0.06 eV.

For 0.5ML and 0.75 ML coverages, we found new configurations with mixed CO binding sites, with lower energies than the data in the parameterization set. The lowest energy configuration we found for 0.5 ML coverage is an equal mix of atop and bridge sites. This configuration is consistent with a previous STM study of the CO adsorption pattern [4]. The lowest energy configuration for 0.75 ML coverage mixes atop and three-fold binding in a 1:2 ratio (see below). In figure 1b, we plot all the DFT energies as a function of coverage. We can see the energy decreases linearly up to 0.50 ML, beyond which non-linearity develops. This is also manifested in figure 1c, where the differential binding energy curve shows a sudden decrease. We had added in the zero point energy corrections when constructing the differential binding energy curve. The sharp decrease in the differential binding energy at 0.5 ML and 0.75 ML has also been observed in experiments [1].

The ground state geometries for the predicted intermediate coverages are shown in figure 2b. The adsorbed CO is generally uniformly distributed on the surface to minimize their lateral repulsions. By using the *p*(4x4) unit cell, we were able to explore more adsorption patterns than those compatible with a smaller *c*(2x4) or *p*(2x2) unit cell. Our combined MC simulations with DFT verification greatly enhanced our probability of capturing the correct ground state. For example, previous literature [14] reports 0.50 ML is energetically lower than 0.75 ML, which is largely due to the artifact of the small *c*(2x4) unit cell the authors had adopted in the simulation. In our case, the ground state we found at 0.75 ML is much lower in energy compared to the literature geometry, making 0.75 ML coverage thermodynamically more favorable than 0.50 ML. The maximization of CO the inter-molecular distance (and thus minimization of total energy) also eliminates the reported CO adsorption barrier at 0.75 ML [14].

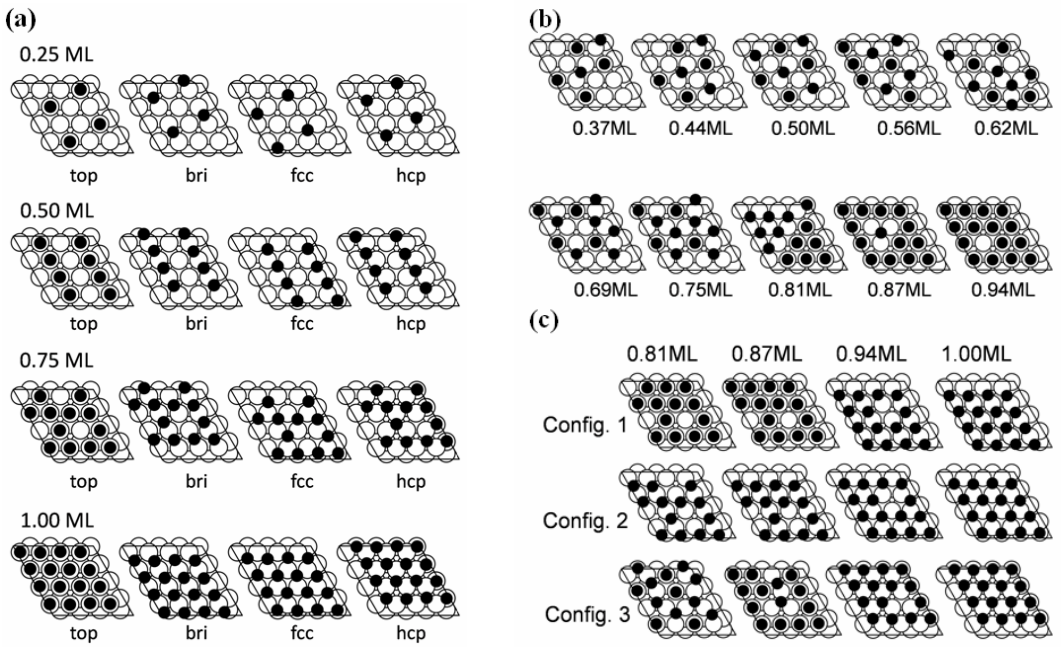

Figure 2. (a) CO adsorption configurations considered at 0.25ML, 0.5ML, 0.75ML and 1ML, respectively. (b) the determined ground states combining Monte-Carlo and DFT calculations (c) Additional high energy states configurations included in fitting the metal sharing model.

In Model I & II, some of the high energy configurations were notable outliers in the fit. This is likely due to the effects of metal sharing. It is possible to quantitatively predict these higher energy states by extension of the current model. With additional higher energy configurations (figure 2c), we fitted Model III in which an energetic penalty for metal-metal sharing is explicitly included. The more sophisticated classical potential is

$$E_{tot} = n_A \Delta E_{top} + n_B \Delta E_{bri}(N) + n_F \Delta E_{fcc}(N) + n_H \Delta E_{hcp}(N) + \frac{1}{2}\sum_{i,j}^{N} \alpha \exp[-\beta(R_{ij} - r_0)]$$

where $\Delta E_i(N) = \Delta E_i^0 + N \cdot \delta$, *i=bri, fcc, hcp* and *N* is the number of neighboring COs sharing at least one metal atom ($d < 3.0$ Å), and the other parameters have the same meaning as in Model I & II. The model fits the DFT data well across 35 different configurations with a RMS deviation of 0.18 eV. Table II summarizes the fitted parameters and the statistical quality of different models. The main improvement in fitting the six additional parameters is the better

agreement of high energy states. It does not influence the results of our MC ground state geometries.

CONCLUSIONS

First-principles density functional theory has been used to compute the equilibrium CO adsorption patterns on Pt(111) over a range of coverages. The search for ground state CO adsorption patterns is assisted with an empirical lateral interaction model and MC simulations, which was further validated by DFT calculations. The saturation coverage proposed by DFT calculations and the differential adsorption curve compare well with experiments. The parameterized classical empirical potential can be used in future studies of CO adsorption and oxidation on larger size surfaces using Kinetic Monte Carlo methods. The calculation results increase our understanding of CO saturation adsorption on Pt(111).

REFERENCES

1. G. Ertl, M. Neumann, and K.M. Streit, *Surf. Sci.* **64**, 393 (1977).
2. B.N.J. Persson, M. Tushaus, and A.M. Bradshaw, *Chem. Phys.* **92**, 5034 (1990).
3. H. Steininger, S. Lehwald, and H. Ibach, *Surf. Sci.* **123**, 264 (1982).
4. M.O. Pedersen, M.L. Bocquet, P. Sautet, E. Laegsgaard, I. Stensgaard, and F. Besenbacher, *Chem. Phys. Lett.* **299**, 403 (1999).
5. E.K. Vestergaard, P. Thostrup, T. An, E. Laegsgaard, I. Stensgaard, B. Hammer, and F. Besenbacher, *Phys. Rev. Lett.* **88**, 259601 (2002).
6. S.R. Longwitz, J. Schnadt, E.K. Vestergaard, R.T. Vang, E. Laegsgaard, I. Stensgaard, H. Brune, and F.J. Besenbacher, *Chem. Phys.* **108**, 14497 (2004).
7. S. Desai and M. Neurock, *Elect. Acta.* **48**, 3759 (2003).
8. M. Gajdos, A. Eichler, and J. Hafner, *J. Phys.: Condens. Matter* **16**, 1141 (2004).
9. C. Zhang, P. Hu, and A. Alavi, *J. Am. Chem. Soc.* **121**, 7931 (1999).
10. D.C. Ford, Y. Xu, and M. Mavrikakis, *Surf. Sci.* **587**, 159 (2005).
11. N.V. Petrova, I.N. Yakovkin, and Y.G. Ptushinskii, *Low. Temp. Phys.* **31**, 224 (2005).
12. P.J. Feibelman, B. Hammer, J.K. Norskov, F. Wagner, M. Scheffler, R. Stumpf, R. Watwe, and J. Dumesic, *J. Phys. Chem. B* **105**, 4018 (2001).
13. G. Kresse, A. Gil, and P. Sautet, *Phys. Rev. B* **68**, 073401 (2003).
14. J.A. Steckel, A. Eichler, and J. Hafner, *Phys. Rev. B* **68**, 085416 (2003).
15. W. Kohn, *Rev. Mod. Phys.* **71**, 1253 (1999).
16. B. Hammer, L.B. Hansen, and J.K. Norskov, *Phys. Rev. B* **59**, 7413 (1999).
17. G. Kresse, and J. Furthemuller, *J. Comp. Mat. Sci.* **6**, 15 (1996).
18. P. Blochl, *Phys. Rev. B* **50**, 17953 (1994).
19. S. Kandoi, A.A. Gokhale, L.C. Grabow, J.A. Dumesic, and M. Mavrikakis, *Catal. Lett.* **93**, 93 (2004).
20. N. Metropolis, A.W. Rosenbluth, M.N. Rosenbluth, A.H. Teller, and E. Teller, *J. Chem. Phys.* **21**, 1087 (1953).
21. S. Kirkpatrick, C.D. Gelatt Jr., and M.P. Vecchi, *Science* **220**, 671 (1983).